Int J Appl Earth Obs Geoinformation 63 (2017) 78–89

Contents lists available at ScienceDirect

Int J Appl Earth Obs Geoinformation

journal homepage: www.elsevier.com/locate/jag

Research Paper

Scattering property based contextual PolSAR speckle filter

Adugna G. Mullissa*, Valentyn Tolpekin, Alfred Stein

Department of Earth Observation Science, Faculty of Geoinformation Science and Earth Observation, University of Twente, 7500AE Enschede, The Netherlands

ARTICLE INFO

Keywords:
Polarimetric synthetic aperture RADAR (PolSAR)
Speckle filtering

ABSTRACT

Reliability of the scattering model based polarimetric SAR (PolSAR) speckle filter depends upon the accurate decomposition and classification of the scattering mechanisms. This paper presents an improved scattering property based contextual speckle filter based upon an iterative classification of the scattering mechanisms. It applies a Cloude-Pottier eigenvalue-eigenvector decomposition and a fuzzy H/α classification to determine the scattering mechanisms on a pre-estimate of the coherency matrix. The H/α classification identifies pixels with homogeneous scattering properties. A coarse pixel selection rule groups pixels that are either single bounce, double bounce or volume scatterers. A fine pixel selection rule is applied to pixels within each canonical scattering mechanism. We filter the PolSAR data and depending on the type of image scene (urban or rural) use either the coarse or fine pixel selection rule. Iterative refinement of the Wishart H/α classification reduces the speckle in the PolSAR data. Effectiveness of this new filter is demonstrated by using both simulated and real PolSAR data. It is compared with the refined Lee filter, the scattering model based filter and the non-local means filter. The study concludes that the proposed filter compares favorably with other polarimetric speckle filters in preserving polarimetric information, point scatterers and subtle features in PolSAR data.

1. Introduction

Polarimetric synthetic aperture radar (PolSAR) and polarimetric interferometric SAR (PolInSAR) are useful to estimate physical parameters at the earth surface. The SAR signal is commonly affected by speckle, arising from the coherent superposition of a number of independent scatterers within each resolution cell. If the size of the resolution cell is much larger than the imaging wavelength there will be interference between individual scattering producing speckle. In the presence of speckle the polarimetric response is best taken as a random value. To determine its probability density distribution, second order statistics represented by the polarimetric covariance matrix have to be estimated.

PolSAR speckle filtering and information extraction rely on the applied stochastic model for the PolSAR data. In homogeneous and stationary media, PolSAR data can be characterized by a zero mean multivariate Gaussian pdf (Lee et al., 1994b). The simplest method proposed for reducing speckle is the boxcar filter (Lee, 1980) that estimates the covariance matrix with a moving average operation. The boxcar filter is effective in removing speckle in homogeneous regions at the expense of loss in resolution. To overcome this loss, Lee et al. (1999a) proposed to select similar pixels by using a series of edge aligned non-rectangular windows, Vasile et al. (2006) used intensity driven neighborhood region growing based on the image intensity, Lee et al. (2006) proposed selecting similar neighboring pixels based on scattering characteristics and Lopez-Martinez and Fabregas (2008) suggested an adaptive speckle reduction based on additive and multiplicative noise model. Further, Deledalle et al. (2015) used non-local means with weighted maximum likelihood estimation to reduce speckle, Chen et al. (2011) developed a statistical pre-test method to select homogeneous patches and Zhong et al. (2014) used a statistical testing to establish pixel similarity between two patches that follow a complex Wishart distribution. Most methods, however, focused on pixel statistics without considering pixel scattering properties. An exception was Lee et al. (2006) who considered pixel statistics and polarimetric scattering mechanisms for speckle filtering.

The scattering model based (SMB) speckle filtering method (Lee et al., 2006) applied the Freeman-Durden model based decomposition (Freeman and Durden, 1998) to determine the dominant scattering mechanism power on a pixel by pixel basis. Unsupervised classification is initialized by grouping pixels into clusters for each canonical scattering mechanism. These are merged into classes for each scattering mechanism using a Wishart merge distance measure. This method preserves the dominant scattering mechanisms of each pixel. The following limitations require compensation. First, the Freeman-Durden model based decomposition tends to overestimate the volume scattering component in urban settings (Yajima et al., 2008; Yamaguchi et al., 2011). It assumes that all cross polarized return is due to

* Corresponding author.
E-mail addresses: a.mullissa@utwente.nl (A.G. Mullissa), v.a.tolpekin@utwente.nl (V. Tolpekin), a.stein@utwente.nl (A. Stein).

http://dx.doi.org/10.1016/j.jag.2017.07.011
Received 19 January 2017; Received in revised form 1 July 2017; Accepted 20 July 2017
Available online 01 August 2017

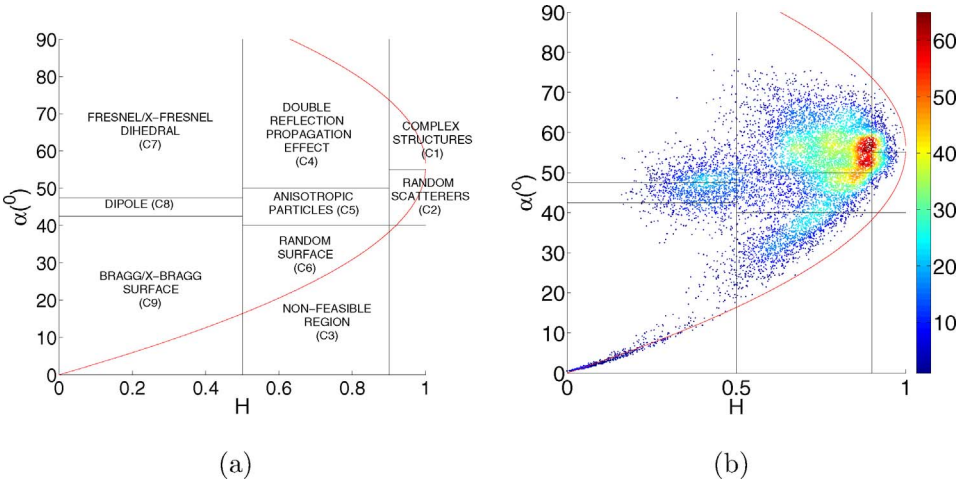

Fig. 1. (a) The H/α plane showing different scattering properties, as defined in Cloude and Pottier (1997), Cloude and Pottier (1996). (b) The H/α density plot derived from a simulated PolSAR data. The color scale indicates the number of pixels per data point. (For interpretation of the references to color in this figure legend, the reader is referred to the web version of this article.)

vegetation. Rough surfaces and local topography, however, can also cause depolarization resulting in a higher cross polarization return in SAR data. Hence, to achieve improved decomposition results from the Freeman-Durden decomposition it is important to correct for the orientation angle. This increases processing time for speckle reduction. Second, clustering the scattering classes into classes for each scattering mechanism implies that pixels that are filtered together belong to the same scattering mechanism. This clustering of pixels is efficient in case of relatively accurate decomposition results and classification of scattering mechanisms. If a pixel is dominated by speckle or if its amplitude level is near the noise floor, decomposition may lead to less accurate results (Wang and Davis, 1997). Hence, subsequent filtering based upon this method of selection will lead to less accurate results. Third, in Lee et al. (2006) the Freeman-Durden decomposition is initialized with a 3×3 pre-estimate of the covariance matrix to estimate the three main scattering mechanisms: single bounce, double bounce and volume. This decomposition is inherently biased when using a small number of pixel samples. Its quantification is in-sufficiently addressed in the literature, although, Lee et al. (2008) evaluated the bias introduced in target decomposition and concluded that parameters of the scattering mechanism are best estimated using at least a 9×9 multi-looking window.

The objective of this paper is to improve the existing SMB speckle filtering method for PolSAR data. It builds upon SMB filtering by addressing the specific limitations listed above. The proposed method uses the Cloude-Pottier eigenvalue-eigenvector decomposition of the coherency matrix to reduce bias in the target decomposition. Both coarse and fine pixel selection are included to minimize the pixel selection error. It also minimizes the scattering mechanism decomposition and classification bias by iteratively increasing the number of looks included in estimating the scattering mechanism and refining the scattering mechanism classification. The method is applied on both simulated data and real PolSAR data acquired from the AIRSAR airborne sensor acquired over Flevoland, The Netherlands and San Franscico, USA.

2. SAR polarimetry

Fully polarimetric SAR sensors measure the scattering matrix (Sinclair matrix) S. For a single pixel it equals:

$$S = \begin{bmatrix} S_{HH} & S_{HV} \\ S_{VH} & S_{VV} \end{bmatrix}, \tag{1}$$

where the complex scattering coefficient S_{XY} indexed as $X, Y = (H, V)$ represents the horizontal (H) and vertical (V) polarization states. In SAR polarimetry, S is represented by the target scattering vector k. Assuming reciprocity i.e. $S_{HV} = S_{VH}$, the linear target scattering vector of a given scattering matrix is given in the monostatic case as:

$$k = [S_{HH} \quad \sqrt{2}S_{HV} \quad S_{VV}]^T \tag{2}$$

where T designates a matrix transpose (Lee and Pottier, 2009).

For deterministic point scatterers k fully describes the scattering process. For distributed scatterers, however, k displays a random property and is modeled (Lee et al., 1994b) by a multivariate complex circular Gaussian probability density function:

$$p_k(k) = \frac{1}{\pi^3 |C|} \exp(-k^\dagger C^{-1} k). \tag{3}$$

Here $C = E\{kk^\dagger\}$ is the covariance matrix, $|C|$ is the determinant and † denotes the complex conjugate transpose. Assuming stationarity and ergodicity in the neighborhood of a pixel, an estimate of the covariance matrix is obtained by:

$$Z = \langle \mathrm{k}\mathrm{k}^\dagger \rangle = \frac{1}{n} \sum_{i=1}^{n} kk^\dagger. \tag{4}$$

where n is the number of looks used to estimate Z. The distribution of Z is modeled by the complex Wishart probability density function (Goodman, 1963). Note that the covariance matrix can be transformed into the coherency matrix T

$$T = (\mathrm{SU}_3) C (\mathrm{SU}_3)^{-1}, \tag{5}$$

where $\mathrm{SU}_3 = \frac{1}{\sqrt{2}} \begin{bmatrix} 1 & 0 & 1 \\ 1 & 0 & -1 \\ 0 & \sqrt{2} & 0 \end{bmatrix}$ is a unitary transformation matrix.

3. Scattering property based contextual speckle filtering

3.1. Scattering mechanism classification

The Cloude-Pottier eigenvalue-eigenvector decomposition (Lee et al., 1999b) is applied to correct for bias caused by the Freeman-Durden decomposition. It is selected because it is able to derive the scattering mechanism (α) and scattering entropy (H) without being affected by differences in the orientation angle and no a-priori scene information is required to derive the scattering mechanism.

Based on H and α values, pixels can be classified into their respective scattering classes. The H/α plane (Fig. 1b), however, reveals continuously distributed H/α values, whereas the class boundaries in Fig. 1a are crisp. Such ambiguity presents a problem of defining class mixtures near the boundaries. To resolve it we implemented a fuzzy H/α classification (Park and Moon, 2007) for the first filtering. This is followed by the Wishart distance classification in the next iterations (Lee et al., 1999b).

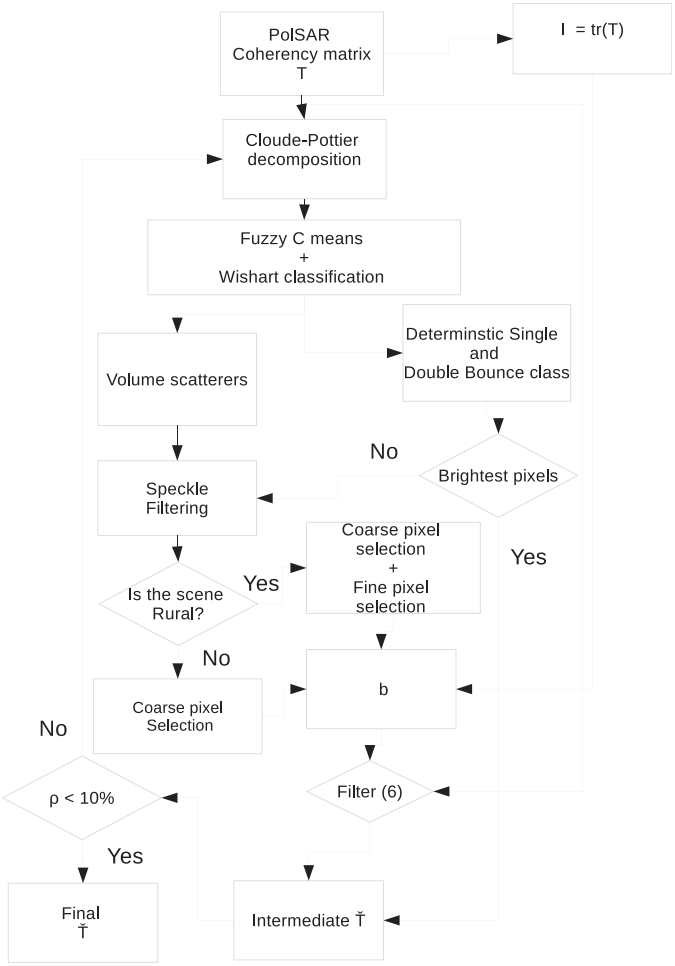

Fig. 2. Methodology flowchart for the proposed method.

3.2. Speckle filtering

We carry out the speckle reduction in two steps. First, we derive the rules that guide the speckle filter. This step is important to minimize the pixel selection bias discussed in Section 1. Second, we iteratively refine the scattering mechanism classification to reduce the estimation of scattering mechanism and classification bias that arises from initializing from a small number of looks while improving the filtering result.

3.2.1. Rule derivation

The fuzzy H/α classification output is defined in the H/α plane, typically resulting in eight scattering classes. The application of the term 'classes' in this context doesn't imply thematic classes. A physical interpretation of the classified output is detailed in Lee and Pottier (2009). Based upon this interpretation, coarse and fine pixel selection are introduced. Coarse pixel selection groups the scattering classes into single bounce, double bounce and volume scattering mechanisms. The canonical scattering mechanisms are derived from the fuzzy H/α classification output using the procedure described in Ferro-Famil et al. (2002). Hence, pixels grouped as single bounce scattering are un-filtered from pixels grouped as double bounce or volume scattering. Similarly, pixels grouped as double bounce and volume scattering remain separate from other groups to preserve the dominant scattering mechanism of the pixel. The brightest pixels within the single bounce and double bounce group larger than a 9 pixel patch are un-filtered i.e. they keep their original pixel values in order to remove isolated deterministic point scatterers. Fine pixel selection does not group the scattering classes to their main scattering mechanisms, i.e. pixels from the eight scattering types remain separate from other classes. Hence, they are filtered separately even if pixels share the same canonical scattering mechanism. The brightest pixels from Class 7 (deterministic dihedral scattering) and Class 9 (Bragg scattering) larger than a 9 pixel patch remain un-filtered, whereas the other scattering types are filtered from pixels within the same scattering class.

Depending upon the image scene environment (urban or rural) we can either use coarse selection, fine selection or a combination of the two to obtain the optimal output. For pixels thus selected, we use the local minimum mean squared error estimator (LMMSE) that is commonly used to estimate the filtered coherency matrix (Lee et al., 1999a). Depending on the applied selection rule, pixels within the filter window belonging to the same scattering type are therefore filtered as:

$$\tilde{T} = \langle T \rangle + b(T - \langle T \rangle). \quad (6)$$

Here $\tilde{T}$ is the result of speckle filtering and $\langle T \rangle$ is the average single look coherency matrix of pixels with the same scattering class as

Table 1
Reference coherency matrix ($\tilde{T}$) for each simulated scattering class (Foucher and Lopez-Martinez, 2014). The coherency matrix in C7 is rank 1 so α, H and A are not defined.

Scattering class	Coherency matrix	α	H	A
C1	$\begin{bmatrix} 5.56 & -0.03-0.36i & 0.47-0.24i \\ -0.03+0.36i & 6.64 & 0.24-0.20i \\ 0.47+0.24i & 0.24+0.20i & 4.53 \end{bmatrix}$	56.6°	0.98	0.14
C2	$\begin{bmatrix} 7.79 & -0.03-0.50i & 0.56-0.30i \\ -0.03+0.50i & 5.38 & 0.20-0.17i \\ 0.56+0.30i & 0.20+0.17i & 4.38 \end{bmatrix}$	50.1°	0.97	0.12
C4	$\begin{bmatrix} 14.69 & 2.59-0.92i & 1.98-0.85i \\ 2.59+0.92i & 25.39 & 4.55+0.20i \\ 1.98+0.85i & 4.55-0.20i & 5.12 \end{bmatrix}$	57.8°	0.8	0.57
C5	$\begin{bmatrix} 10.95 & 0.420-0.89i & 1.17-0.65i \\ 0.420+0.89i & 7.51 & 0.83 \\ 1.17+0.65i & 0.83 & 3.29 \end{bmatrix}$	45.7°	0.89	0.42
C6	$\begin{bmatrix} 10.99 & -0.45-0.69i & 0.85-0.73i \\ -0.45+0.69i & 3.38 & 0.21+0.01i \\ 0.85+0.21-0.01i & 2.05 & \end{bmatrix}$	32.8°	0.76	0.28
C7	$\begin{bmatrix} 990.02 & 4.97 & 7.04 \\ 4.97 & 0.02 & 0.04 \\ 7.04 & 0.04 & 0.05 \end{bmatrix}$	–	–	–
C8	$\begin{bmatrix} 29.95 & 23.04+0.79i & 4.83-2.47i \\ 23.04-0.79i & 29.99 & 5.21-3i \\ 4.83+2.47i & 5.21+3i & 3.23 \end{bmatrix}$	46.9°	0.44	0.57
C9	$\begin{bmatrix} 5.40 & -1.14-0.34i & 0.27-0.33i \\ -1.14+0.34i & 0.56 & -0.01-0.09i \\ 0.27+0.33i & -0.01-0.09i & 0.16 \end{bmatrix}$	18.3°	0.26	0.4

Table 2
MRF image morphology simulation parameters.

Parameter	Value
Prior energy model	Potts model
Neighbourhood system	Second order with inverse distance weights
Number of iterations	200
Cooling schedule	$T_{k+1} = T_k \cdot \sigma$ where $T_o = 10$ and $\sigma = 0.9$
Starting point	Uniform random
Point scatterers	Randomly added

defined in the filtering rule and b is a weight assigned during filtering. This weight is derived from the total backscattered power $I = tr(T)$ (Lee et al., 1999a) and evenly applied to each component of T. This procedure is based upon the assumption that the noise is multiplicative, with unity mean that is uncorrelated with the image.

3.2.2. Iterative refinement

The filtering procedure described in the preceding section is initialized using a 3 × 3 window for single look datasets. If the input PolSAR coherency matrix is a rank 3 matrix we can decompose and classify without further averaging. The success of filtering depends upon accurately determining and interpreting the scattering mechanism and an accurate classification of the scattering type. As shown in Lee et al. (2008), estimates of both H and α are close to their true value if the number of looks equals 81 or above. Unfortunately, point scatterers are smoothed when initializing with such a large window size. To correct for this, we initialize with the 3 × 3 window average to obtain the approximate H/α values and the initial fuzzy H/α classification of the scattering types and gradually increase the filter window size to preserve point scatterers while improving the scattering mechanism estimate and classification output. This classification output is used to adaptively filter the single look T. Next, we use the adaptively filtered covariance matrix to derive new H/α values and a new Wishart distance classification output. We then use the Wishart classification output to adaptively filter the single look T using a 5 × 5 window. This procedure is repeated until the desired window is reached and the number of pixels that switch scattering classes is below a threshold ρ. In this study a $\rho < 10\%$ is used. For most data it takes 4–6 iterations for the filtering process to terminate. We used an 11 × 11 final window to have sufficient pixels for effective filtering. The methodology flowchart for the proposed method is given in Fig. 2.

4. PolSAR data simulation

Speckle is present in virtually all SAR data. Accurate quantitative evaluation of speckle filtering is only possible if a noise free image is available, which is the case for simulated images. Hence, to apply quantitative evaluation of the proposed speckle reduction method we adapted the Monte-Carlo PolInSAR simulation routine proposed by Cloude (2010) to PolSAR data. In addition, we reproduced the complex image structure in real PolSAR data by simulating a random image morphology.

Following (3) we assumed that the stochastic nature of the scattering vector k is completely determined by the covariance matrix C. We first defined a coherence matrix to be used as a reference. Since the

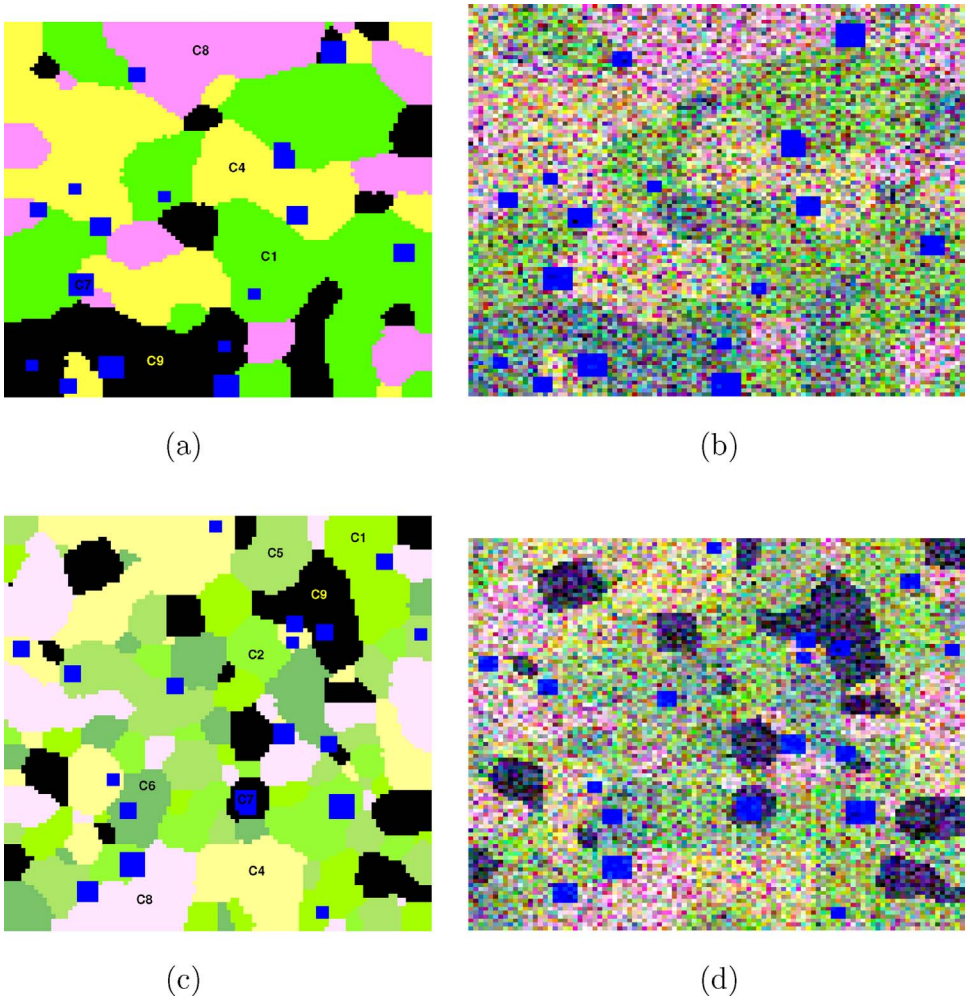

Fig. 3. Pauli images of simulated PolSAR data. (a) Reference image derived from five scattering classes. The corresponding scattering classes are labeled as defined in Table 2. (b) Simulated PolSAR data derived for five scattering classes. In the images red color represents $|S_{HH} - S_{VV}|^2$, blue color represents $|S_{HH} + S_{VV}|^2$ and green color represents $|2S_{HV}|^2$. (c) Reference image derived from eight scattering classes. The corresponding scattering classes are labeled as in Table 2. (d) Simulated PolSAR data with the same color as in (b). (For interpretation of the references to color in this figure legend, the reader is referred to the web version of this article.)

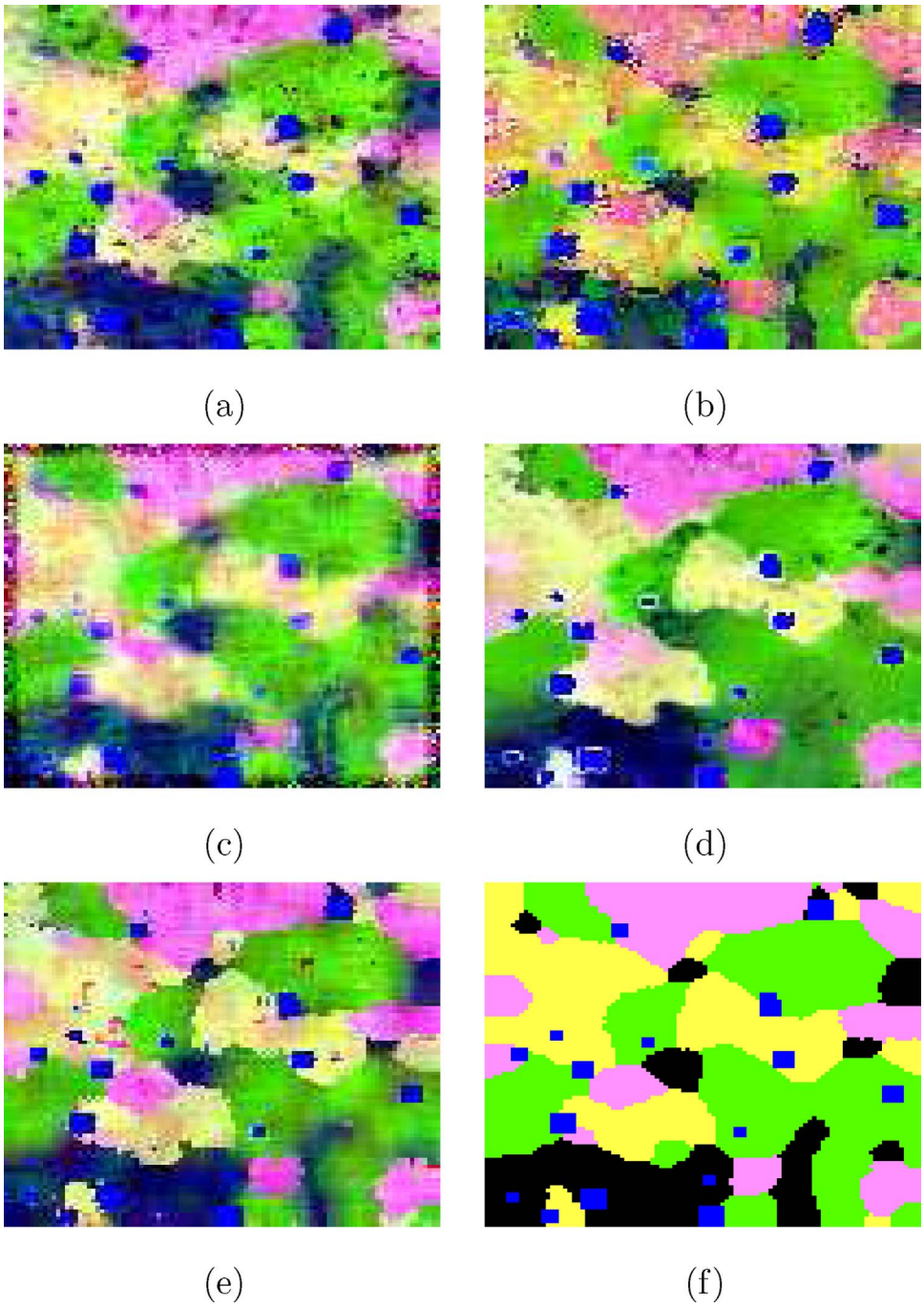

Fig. 4. Speckle filtering results of false color composite in Pauli basis based on simulated data. The speckle free and speckled simulated data is shown in Fig. 2. (a) Pauli channels created from IDAN filter using window size row of 80 (b) Pauli channels created from Scattering model based filter with 9 × 9 window. (c) Pauli channels for Refined lee filter with 9 × 9 window. (d) Pauli channel for Non-local means with 21 × 21 search window, patch size of 5 × 5 and threshold coefficient = 20. (e) Pauli channel for proposed method 11 × 11 window 5 iteration. (f) Pauli channel for the ground truth image.

coherency matrix is a Hermitian positive semi-definite matrix, we factorized the reference coherency matrix $\widetilde{T}$ to its respective eigenvalues and eigenvectors.

$$\widetilde{T} = U\Sigma U^{\dagger}. \tag{7}$$

Here, U contains the eigenvectors arranged in columns and Σ is a diagonal matrix containing the corresponding eigenvalues λ. The eigenvalues and eigenvectors generate a sequence of n dimensional complex vectors k, with coherency matrix T. We next generated two independent real random sequences following Gaussian distributions, G_a and G_b with mean = 0 and variance = 0.5 and combined them into a complex series after scaling it by the square root of the appropriate eigenvalue.

$$e = \{e_j\}, \quad j = 1, \ldots, n, \quad e_j = \sqrt{\lambda_j}\{G_a(0, 0.5) + iG_b(0, 0.5)\}. \tag{8}$$

Next, we generated k by collecting G_a and G_b into a vector e and introducing a complex correlation by multiplying this vector with the matrix of eigenvectors, i.e. $k = U \cdot e$. The vector k follows a zero mean complex multivariate Gaussian pdf as in (3).

Finally, we generated a random image morphology with different features, by using different $\widetilde{T}$ matrices for different scattering classes extracted from the four look AIRSAR data (Table 1). We used a Markov random field (MRF) following the Gibbs distribution (Boykov et al., 2001). The parameters used to simulate a random image morphology are shown in Table 2.

As stated in different speckle filtering literature, a speckle filter is supposed to remove speckle noise from distributed scatterers while preserving edges and point scatterers in a PolSAR image. Hence, the selection of a deterministic scatterer class and a varying number of distributed scatterers is reasonable for the evaluation of PolSAR speckle

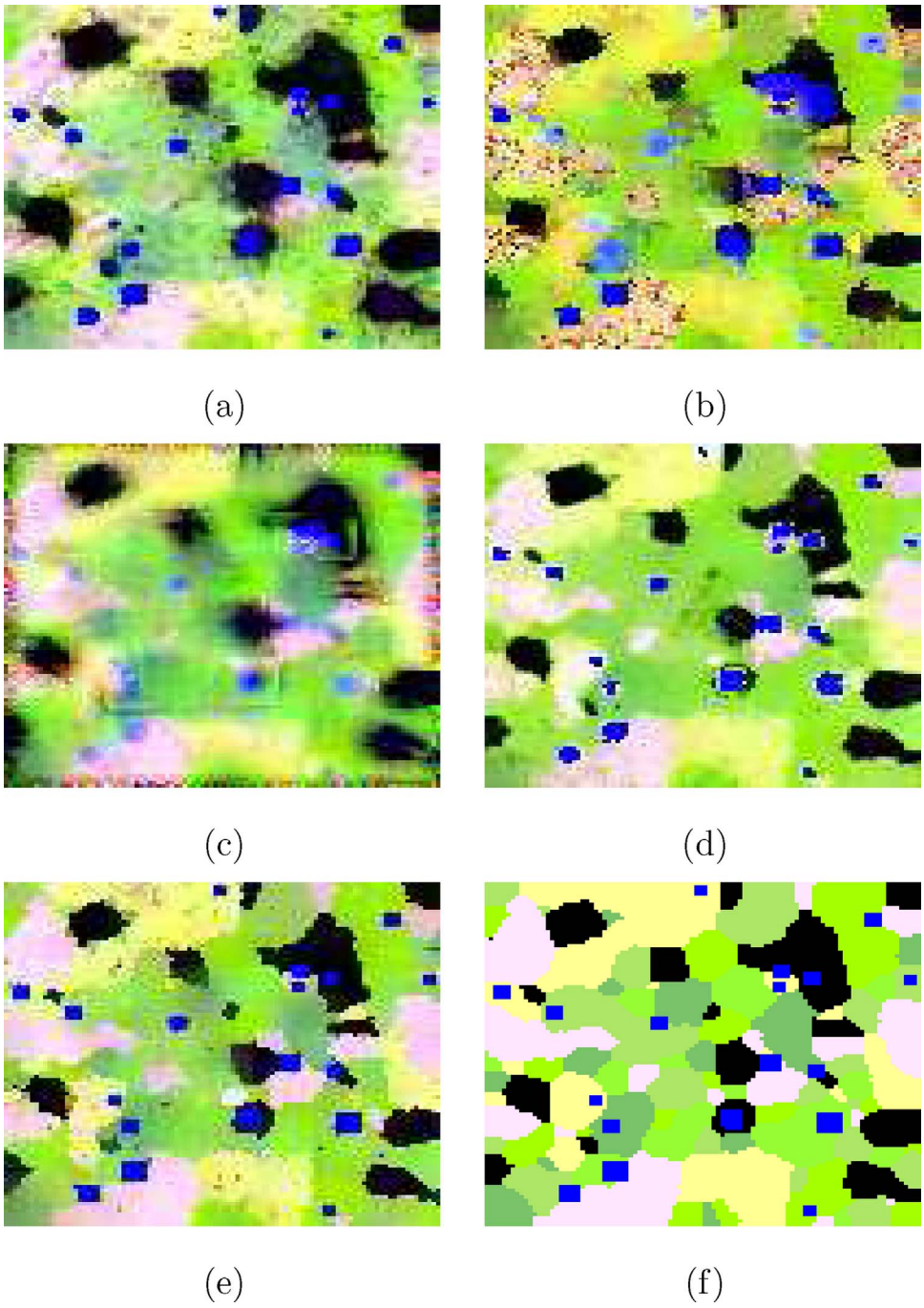

Fig. 5. Speckle filtering results of false color composite in Pauli basis based on simulated data from 8 scattering classes. The speckle free and speckled simulated data is shown in Fig. 2. (a) Pauli channels created from IDAN filter using window size row of 80 (b) Pauli channels created from Scattering model based filter with 9 × 9 window. (c) Pauli channels for Refined lee filter with 9 × 9 window. (d) Pauli channel for Non-local means with 21 × 21 search window, patch size of 5 × 5 and threshold coefficient = 20. (e) Pauli channel for proposed method 11 × 11 window 5 iteration. (f) Pauli channel for ground truth image.

filters. Two simulated images were generated by taking five scattering classes (Fig. 3a) and eight scattering classes (Fig. 3c). Of these classes one represents a deterministic Point scatterer and the others represent a distributed scattering with different α and H values. Speckle was added to the distributed scattering classes using (8) but no speckle was added to the deterministic point scatterers.

5. Datasets

To test the performance of the proposed method in addition to the simulated data, real airborne SAR data from the JPL/NASA AIRSAR airborne polarimetric SAR sensor (Figs. 6a and 7a) was used. The AIRSAR sensor acquires fully polarimetric data in C, L and P band. In this study the L band was selected to evaluate the proposed speckle filtering method. A 1024 × 900 subset of AIRSAR data of San Francisco, USA covers mostly urban area whereas a 1024 × 750 subset of Flevoland, Netherlands covers almost entirely rural land. The acquisition parameters for the AIRSAR sensor are summarized in Table 3. The ground truth data from 14 feature types for the Flevoland scene was adopted from Lee et al. (2001).

6. Results

6.1. Simulated data

To quantitatively evaluate the performance of the different speckle filtering methods, we calculated the absolute error introduced from different speckle filtering methods. Error is defined as the deviation of an estimated parameter from its true value. The average error of α for simulated scattering class (i) is obtained as $\text{Error}(i) = \text{mean}\{|\tilde{\alpha}(i) - \alpha(i)|\}$,

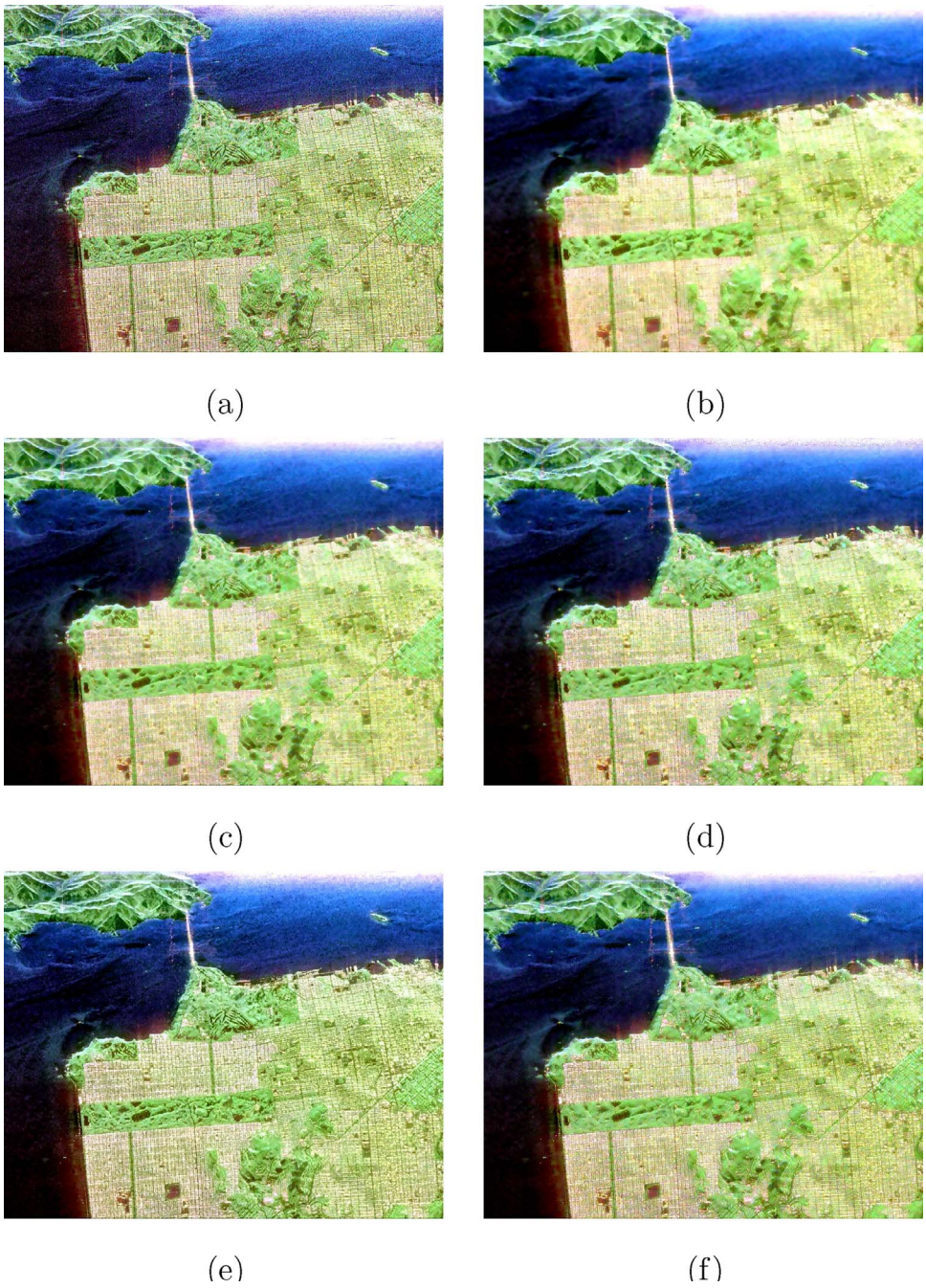

Fig. 6. Speckle filtering results of false color composite in Pauli basis based on AIRSAR airborne L band data acquired over San Francisco. (a) Original 4 look SAR data (b) 80 window row IDAN filter. (c) Refined lee filter with 9 × 9 window. (d) Scattering model based filter with 9 × 9 window. (e) Non-local means with 21 × 21 search window, patch size of 5 × 5 and threshold coefficient = 20. (f) Proposed method 11 × 11 window 5 iteration.

where $\alpha(i)$ is the estimated physical scattering mechanism and $\tilde{\alpha}(i)$ is the reference scattering mechanism. Similar equations apply to the bias of H and A, respectively. The proposed method compares favorably with the other speckle filters in preserving polarimetric information (Tables 4 and 5).

Next, we determined the equivalent number of looks (ENL) for each distributed scattering class, $\mathrm{ENL}(i) = \left(\frac{\zeta(i)}{\tau(i)}\right)^2$, where $\zeta(i)$ is the mean and $\tau(i)$ is the standard deviation of W for class i and took the average of individual class ENL values. High ENL values indicate a better performance of removing speckle from homogeneous regions. The proposed method compares favorably with all other evaluated methods with respect to the described 5 accuracy measures in reducing speckle from homogenous regions.

To evaluate the edge preservation ability of the proposed method we implemented the edge preservation index (*EP*) as detailed in Foucher and Lopez-Martinez (2014). We first defined the gradient preservation index (*GP*), derived by taking the average ratio between the observed gradient values on the filtered Span image I to the gradient on the reference Span image $\tilde{I}$.

$$\mathrm{GP} = \frac{1}{\nu} \sum_{l=1,\ldots,\nu} \frac{\sum_{L(x)=l,|\nabla\tilde{I}(x)|>0} |\nabla I(x)|}{\sum_{L(x)=l,|\nabla\tilde{I}(x)|>0} |\nabla\tilde{I}(x)|}. \tag{9}$$

Here, ∇ is the Sobel gradient operator, $L(x)$ is the class label for pixel x and ν is the number of distributed scattering classes. *EP* is derived by projecting the values of *GP* in the interval [0, 1] using the triangular function given as:

$$\mathrm{EP} = \begin{cases} 1 - |1 - \mathrm{GP}|, & \mathrm{GP} < 2. \\ 0, & \mathrm{GP} \geq 2. \end{cases} \tag{10}$$

We took the average for each scattering class to evaluate the overall

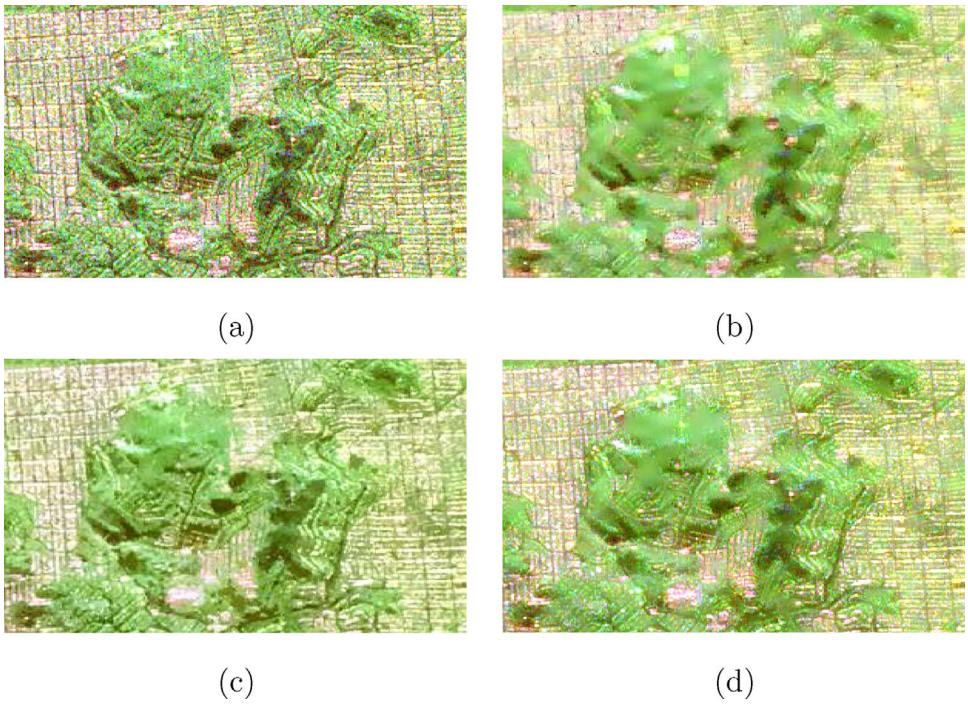

Fig. 7. Speckle filtering of a subset of 300 × 235 pixels from the AIRSAR San Francisco bay image. (a) Original 4 look data. (b) Scattering model based filter with 9 × 9 window. (c) Non-local means with 21 × 21 search window, patch size of 5 × 5 and threshold coefficient = 20. (d) New method 11 × 11 window 5 iteration.

Table 3
JPL/NASA AIRSAR airborne polarimetric SAR sensor acquisition parameters.

Parameter	Value
Sensor	AIRSAR airborne sensor
Frequency/wavelength	1.26 GHz/23 cm
Polarization	Full
Range resolution	3.75 m
Swath width (nominal)	10 km
Off-Nadir angle (normal)	20–60°

Table 4
The absolute error in α, H and A estimates from using different speckle filtering methods and the ENL and EP calculated from different speckle filtering methods on simulated five scattering class PolSAR data. The error values for α are in degrees.

Method	α	H	A	ENL	EP
IDAN	2.109	0.05	0.068	14.32	0.904
Lee	3.1716	0.072	0.137	5.861	0.9518
SMB	1.554	0.053	0.118	1.4828	0.6233
NL	4.373	0.0649	0.103	7.4298	0.9827
New	1.6817	0.022	0.0428	15.014	0.978

Table 5
The absolute error in α, H and A estimates from using different speckle filtering methods and the ENL and EP calculated from different speckle filtering methods on simulated eight scattering class PolSAR data. The error values for α are in degrees.

Method	α	H	A	ENL	EP
IDAN	3.374	0.073	0.075	12.621	0.92
Lee	3.838	0.095	0.126	3.987	0.8463
SMB	2.353	0.095	0.1175	0.296	0.3476
NL	4.223	0.073	0.09	5.895	0.8516
New	2.208	0.0419	0.066	9.836	0.9706

edge preserving performance. Low values of *EP* indicate edge over-filtering or under filtering, whereas a high *EP* value indicates a good edge preservation. We observe that the proposed method performs well in preserving edges in both simulated data.

To investigate the efficiency of the proposed filter an image profile was created to compare $|S_{HH} + S_{VV}|^2$ intensity profile with the other state of the art filtering methods (Fig. 9). The new filter achieves the best filtering results as compared with the true $|S_{HH} + S_{VV}|^2$ intensity. The non-local means and the proposed method adequately remove speckle while maintaining determisitic point scatterers, whereas the poor edge preservation performance of SMB is clearly indicated in Fig. 9a.

Table 6
Speckle filtering methods and their respective computational efficiency measured per pixel when run using an Intel Core i7 CPU with 8 GB memory run on a 64 bit Linux environment.

Method	Computation time, s
IDAN	3.97×10^{-5}
Refined Lee	4.02×10^{-5}
SMB	1.99×10^{-4}
NL	2.72×10^{-4}
Proposed method (coarse selection, 5 iterations)	2.1×10^{-3}
Proposed method (fine selection, 5 iterations)	6×10^{-3}
Proposed method (coarse (2 iterations) and fine selection (3 iterations))	4.4×10^{-3}

6.2. Airborne AIRSAR data

Figs. 6 and 8 show that the IDAN filter performs well in preserving edges but it didn't fully remove the speckle noise found around volume scatterers. SMB was not successful in preserving point scatterers and edges. Furthermore, it introduced artifacts throughout the image (Fig. 8c). The refined Lee filter preserved strong point scatterers but smoothened out other point scatterers. The non-local means had a variety of results when used in conjunction with the refined Lee and Lee sigma filter (Lee et al., 2009). It preserved point scatterers but a general over-filtering is observed when used with refined Lee filter. It achieved its best result when used with the Lee sigma filter with a 21 × 21 search window, 3 × 3 target search window, patch size of 5 × 5, a 9 × 9 general filter window and a threshold coefficient equal to 20. The proposed method, was successful in preserving point scatterers and edges while reducing speckle noise using an 11 × 11 window and 5 iterations.

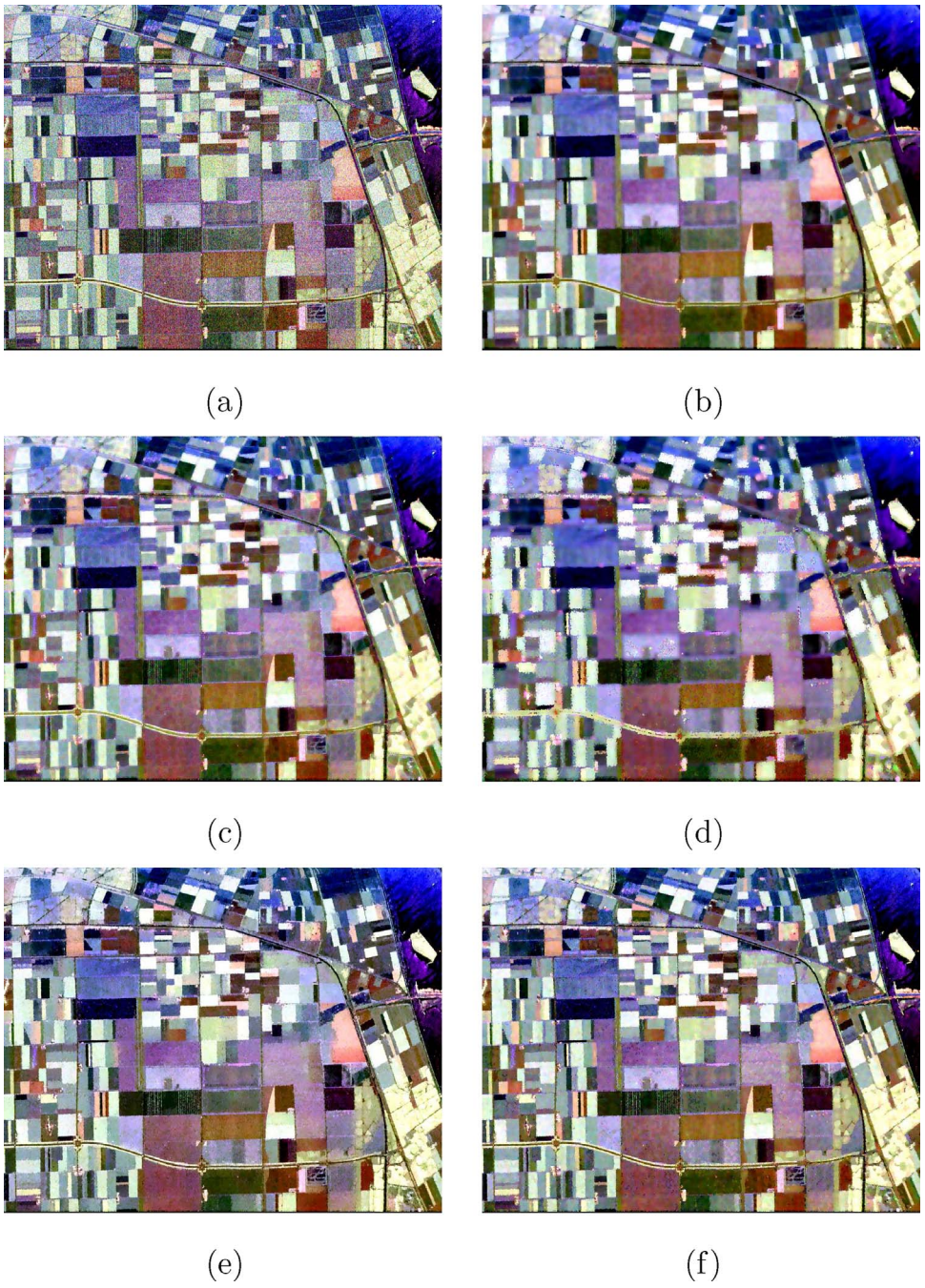

Fig. 8. Speckle filtering results of false color composite in Pauli basis based on AIRSAR airborne L band data acquired over Flevoland, Netherlands. (a) Original 4 look SAR data. (b) 80 window row IDAN filter. (c) Refined lee filter with 9 × 9 window. (d) Scattering model based filter with 9 × 9 window. (e) Non-local means with 21 × 21 search window, patch size of 5 × 5 and threshold coefficient = 20 (f) Proposed method 11 × 11 window 5 iteration.

For AIRSAR data two separate experiments were conducted in a completely rural scene over Flevoland, and a mixture of urban and natural over San Francisco bay region. The refined Lee and scattering model based filters blurred the edges between different agricultural land parcels and roads (Fig. 8). The non-local means filter and the new method both preserved edges while reducing speckle. The non-local means and the new method performed well in reducing speckle while preserving the boundaries between different agricultural land parcels while slight over-filtering was observed on built-up found in the farm lands. In this regard, the new method performed well in preserving the isolated built up features in the image. In the San Francisco bay scene (Fig. 7), the scattering model based filter produced better preservation of points and edges. However, subtle image features were still over filtered. The non-local means filter performed well in preserving edges but it also over filtered built up features that are mixed with vegetation whereas the proposed filter preserved these mixed features.

The proposed method compared favorably with other state of the art speckle filters in preserving point scatterers and edges, even though a block effect is observed around edges because the filter was initialized using a 3 × 3 boxcar average. The non-local means filter (NL) also performed well in preserving points but it showed some deficiency in maintaining edges near feature boundaries. The refined Lee filter failed to preserve many point scatterers and resulted in over-filtering in all regions. The scattering model based filter (SMB) blurred all point scatterers and edges and the IDAN filter preserved the points but failed to filter out the speckle noise from homogeneous regions (Figs. 6 and 8).

6.3. *Effect of speckle filtering for thematic applications*

To evaluate the performance of the proposed speckle filter we applied thematic classification to speckle filtered PolSAR data from different speckle filters and compared the classified output with ground

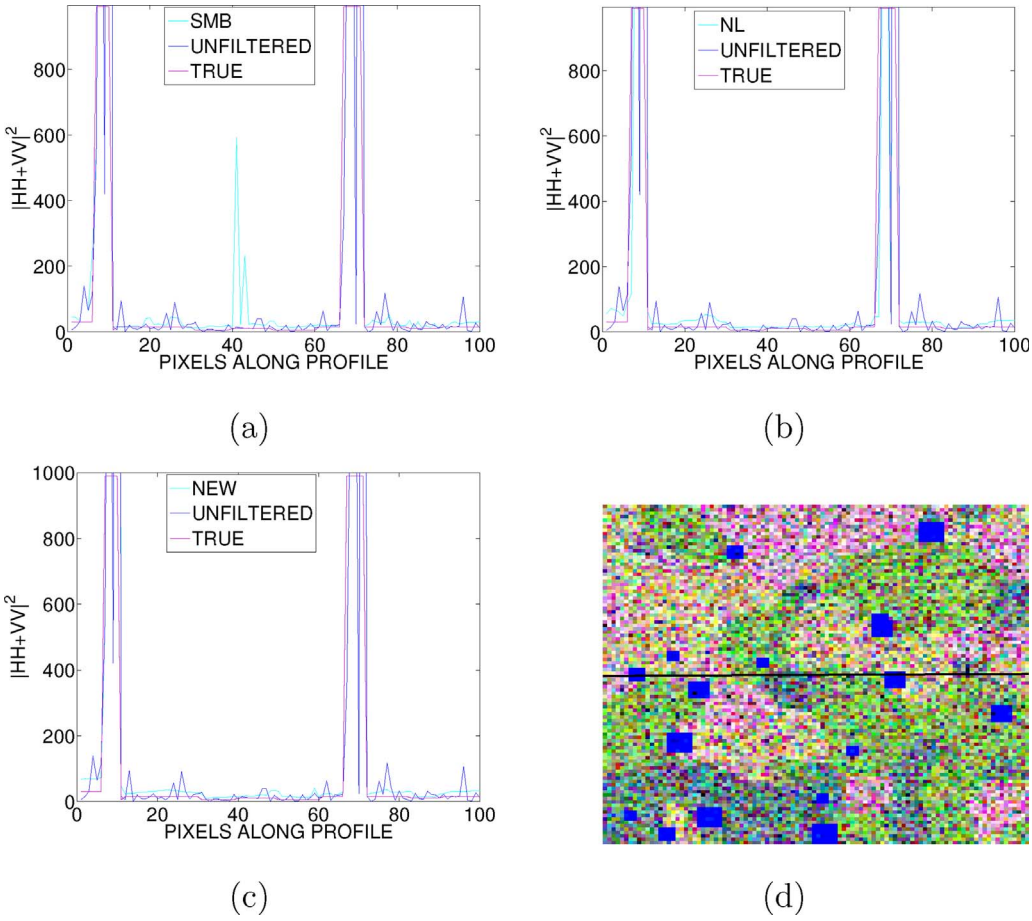

Fig. 9. Intensity profile from simulated data for $|S_{HH} + S_{VV}|^2$ for the different speckle filters as compared with the original unfiltered data and the ground truth image. (a) Scattering model based filter. (b) Non-local means filter. (c) Proposed method. (d) Location where the profile was taken.

Table 7
The classification accuracy for the speckle filtered PolSAR data using different methods.

Method	Observed accuracy	Kappa coefficient
IDAN	0.9161	0.9084
Refined Lee	0.9181	0.9105
SMB	0.9132	0.9051
NL	0.9045	0.8954
Proposed method	0.9074	0.8987

truth data adopted from Lee et al. (2001). Before applying classification we split the ground truth data into training area and a test area. A supervised Maximum Liklihood Wishart distance classifier (Lee et al., 1994a) was implemented on the IDAN, refined Lee, SMB, NL and the proposed method were applied.

It can be observed from Table 7 that the classification accuracy of the proposed method is slightly lower than that of IDAN, refined Lee and SMB. This is due to the generalized feature type indicated by the ground truth (Fig. 10), which differs slightly from the signal variation from the PolSAR data. NL and the proposed method were both designed to preserve spatial details in the PolSAR image. This results in deviation from the generalized ground truth image. To improve the classification accuracy for the proposed method it is recommended to use a larger than 11 × 11 window.

To analyze the effect of speckle filtering on urban scatterers we analyzed the canonical scattering mechanisms from the AIRSAR San Francisco scene. We selected a 100 × 100 patch from the image scene that was built up. We applied Cloude-Pottier eigenvalue and eigenvector decomposition and the unsupervised Wishart classification to derive the scattering mechanisms from speckle filtered PolSAR data. A ratio analysis of the scattering contribution from the three canonical scattering mechanisms after applying different speckle filters was derived.

It can be observed from Table 8 that the proposed method preserves the double bounce component better than the other speckle filtering methods. Different thematic application require different levels of filtering. As indicated in Table 7 thematic applications involving agriculture and forestry require more filtering hence preservation of subtle variations may not be important. With the exception of precision agriculture. On the contrary, urban applications such as characterization of urban scattering often requires preservation of resolution. Hence the optimal speckle filter should perform well in both applications. In this regard, the proposed speckle filter achieved good result. A future study should further analyze the effect of speckle filtering on different thematic applications.

7. Discussion

The proposed method works well with L band PolSAR data. It should be further evaluated for application with short wavelength SAR data in particular for X band high resolution airborne PolSAR data. For instance, the rule deriving the assignment of scattering classes for filtering should be adjusted when using short wavelength high resolution sensors because pixels defined as surface scatterers in L band will be volume scatterers in X band.

We selected the Cloude-Pottier eigenvalue-eigenvector decomposition to replace the Freeman-Durden model based decomposition to minimize the a-priori information requirement in the image scene and minimize the bias from the decomposition method. The Cloude-Pottier eigenvalue-eigenvector decomposition is also roll invariant. Hence, an extra processing step of orientation angle compensation is not required. To minimize the pixel selection bias we applied the fine pixel selection

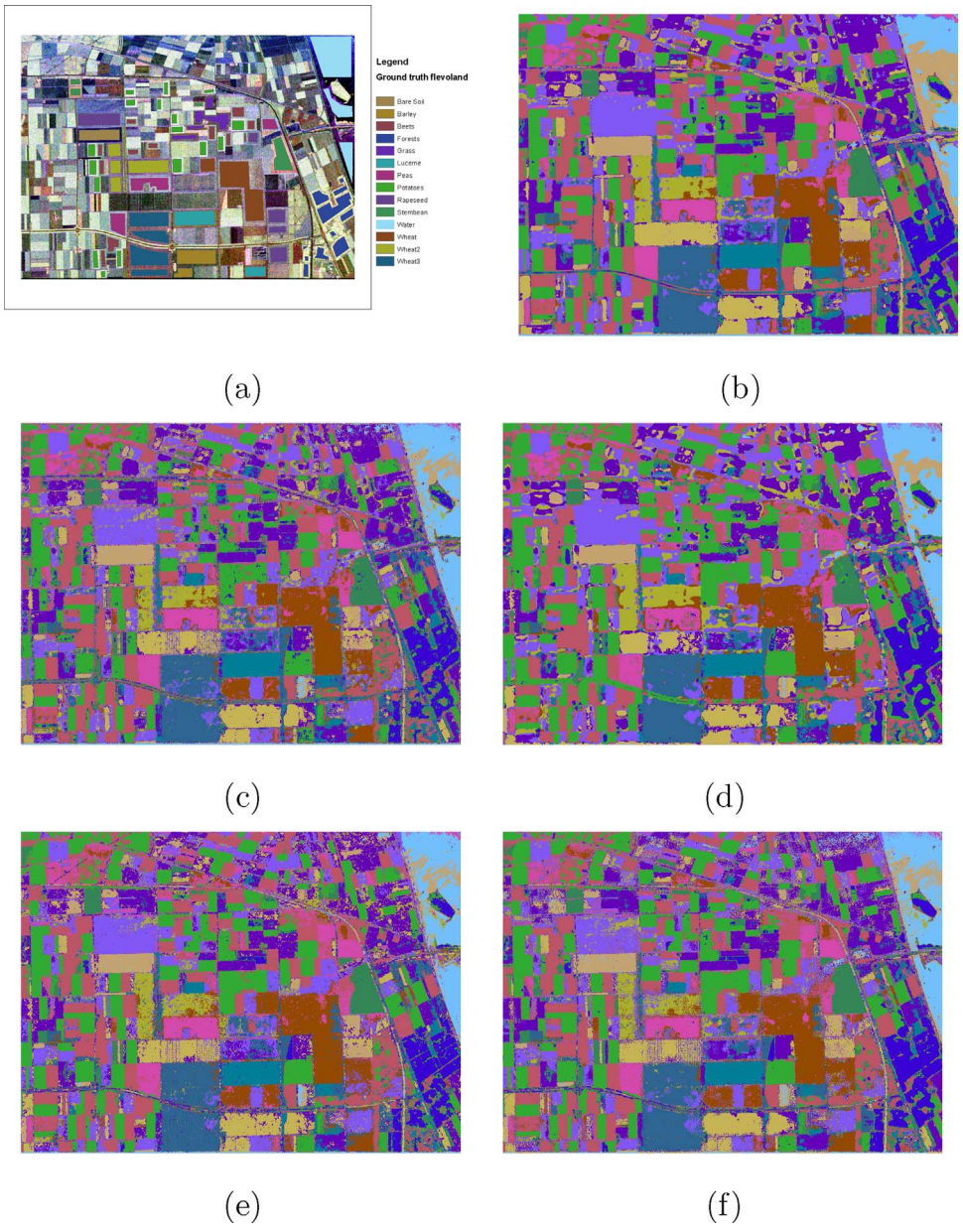

Fig. 10. Supervised Wishart classification of AIRSAR airborne L band data acquired over Flevoland, Netherlands. (a) Ground truth data adopted from Lee et al. (2001), (b) IDAN filter, (c) Refined Lee filter, (d) SMB, (e) and NL (f) proposed method.

Table 8
Scattering mechanism contribution after application of different speckle filtering methods.

Method	Single bounce	Double bounce	Volume
Refined Lee	0.5%	9.91%	89.58%
SMB	1.7%	11.36%	86.93%
NL	0.009%	9.27%	90.71%
Proposed method	1.54%	12.16%	86.28%
4 look original data	2.46%	18.34%	79.19%

in volume scatterers in which all pixels with different scattering properties are not filtered with each other. In addition, MMSE is applied to all pixels in each scattering category which resulted in better preservation of edges in volume scatterers. To mitigate the bias introduced by using a small number of samples in estimating the scattering mechanisms and classification we adopted an iterative decomposition and classification approach. Initializing with a fuzzy H/α classification helped to achieve higher accuracy than crisp Wishart H/α classification. Since speckle level is minimized we applied the crisp Wishart distance classification on subsequent iterations thus maintaining a high classification accuracy while improving computational efficiency. The combination of these three steps resulted in an overall improvement of the speckle reduction results (Figs. 4–8).

The initial fuzzy H/α classification to designate the different scattering mechanisms resulted into improved classification which is critical for a successful application of this method. Fuzzification of the H/α plane led to improved identification and consequent classification of scattering mechanisms. In addition, coarse pixel selection was effective in filtering scenes with a mixture of urban and rural features as in the San Francisco scene. For dominantly rural scenes as in the simulated data and the Flevoland scene, best results were obtained for a mixture of coarse and fine pixel selection. Initial classification of scattering mechanisms was also attempted using the crisp unsupervised Wishart distance classifier (Lee et al., 1999b) and compared with the fuzzy H/α classification. Both classifiers correctly classified surface scatterers (Bragg and random surface scattering) but the unsupervised Wishart classifier underestimated the dihedral scattering component identified on the H/α plane.

The efficiency of the speckle filters for different thematic

applications is different depending on the design parameters of the filter. If the filter is designed to preserve edges it tends to over filter the homogeneous regions in the image thereby more suited for agricultural application. The proposed method was designed to have enough trade off in between smoothing features, preserving edges and point features. Hence, it under performs as compared with IDAN, refined Lee and SMB in thematic applications where spatial variation is un-important as in small scale agricultural applications. This can be mitigated by using a larger than 11 × 11 filter window. In urban thematic applications the proposed method compares favorably with other speckle filters because the filter is designed to preserve polarimetric information, spatial details and point scatterers.

The proposed method has a limitation of achieving good result at the price of computational time (Table 6). This can be prohibitive when processing a large image scene consisting of millions of pixels. This is the main drawback observed from employing the new filtering approach. To reduce the computational time the fuzzy H/α classification can be replaced with the crisp unsupervised Wishart classification at the risk of less accurate scattering type classification output. The proposed technique can be easily extended to filter dual polarization data obtained from sensors such as Sentinel-1. It can also be extended to filter PolInSAR data for coherence estimation. In the current study the scope was limited to qualitative and quantitative evaluation of speckle filtering performance. In future work comparisons should be made with ground truth data to verify the efficacy of the proposed speckle filtering method.

8. Conclusions

The proposed method expands the scattering model based polarimetric speckle filter (Lee et al., 2006). The study shows that the proposed method compares favorably to other methods such as the refined Lee filter, the scattering model based filter and the non-local means filter. We conclude that it performs robustly in a variety of image scenes. However, for small scale agricultural applications it does not perform well. We further conclude that the strength of the proposed method lies in accurately classifying scattering mechanisms that are obtained by iteratively refining the H/α and coherence matrix estimates. Its performance compares favorably with the edge aligned filtering of the refined lee or the patch based Wishart similarity test method implemented in the non-local means filter. The main observed limitation is that it is computationally expensive.

Acknowledgments

This research work was supported by the Ethiopian government under project number INSA9/JT3/1213/13. The authors wish to thank professor Eric Pottier and Dr. Daniele Perissin for the insightful discussions. The authors would also like to express appreciation to the anonymous reviewers for the comments and suggestions, which have improved the quality of the manuscript.

References

Boykov, Y., Veksler, O., Zabih, R., 2001. Fast approximate energy minimization via graph cuts. IEEE Trans. Pattern Anal. Mach. Intell. 23 (11), 1222–1239.
Chen, J., Chen, Y., An, W., Cui, Y., Yang, J., 2011. Nonlocal filtering for polarimetric SAR data: a pretest approach. IEEE Trans. Geosci. Remote Sens. 49 (5), 1744–1754.
Cloude, S.R., Pottier, E., 1996. A review of target decomposition theorems in radar polarimetry. IEEE Trans. Geosci. Remote Sens. 34 (2), 498–518.
Cloude, S.R., Pottier, E., 1997. An entropy based classification scheme for land applications of polarimetric SAR. IEEE Trans. Geosci. Remote Sens. 35 (1), 68–78.
Cloude, S., 2010. Polarisation: Applications in Remote Sensing. Oxford University Press.
Deledalle, C.-A., Denis, L., Tupin, F., Reigber, A., Jäger, M., 2015. Nl-sar: a unified nonlocal framework for resolution-preserving (pol)(in) SAR denoising. IEEE Trans. Geosci. Remote Sens. 53 (4), 2021–2038.
Ferro-Famil, L., Pottier, E., Lee, J., 2002. Classification and interpretation of polarimetric interferometric SAR data. In: IEEE International Geoscience and Remote Sensing Symposium (IGRASS), 2002, vol. 1. IEEE. pp. 635–637.
Foucher, S., Lopez-Martinez, C., 2014. Analysis, evaluation, and comparison of polarimetric SAR speckle filtering techniques. IEEE Trans. Image Process. 23 (4), 1751–1764.
Freeman, A., Durden, S.L., 1998. A three-component scattering model for polarimetric SAR data. IEEE Trans. Geosci. Remote Sens. 36 (3), 963–973.
Goodman, N., 1963. Statistical analysis based on a certain multivariate complex Gaussian distribution (an introduction). Ann. Math. Stat. 34 (1), 152–177.
Lee, J.-S., Pottier, E., 2009. Polarimetric Radar Imaging: From Basics to Applications. CRC Press.
Lee, J.-S., Grunes, M.R., Kwok, R., 1994a. Classification of multi-look polarimetric SAR imagery based on complex Wishart distribution. Int. J. Remote Sens. 15 (11), 2299–2311.
Lee, J.-S., Hoppel, K.W., Mango, S.A., Miller, A.R., 1994b. Intensity and phase statistics of multilook polarimetric and interferometric SAR imagery. IEEE Trans. Geosci. Remote Sens. 32 (5), 1017–1028.
Lee, J.-S., Grunes, M.R., De Grandi, G., 1999a. Polarimetric SAR speckle filtering and its implication for classification. IEEE Trans. Geosci. Remote Sens. 37 (5), 2363–2373.
Lee, J.-S., Grunes, M.R., Ainsworth, T.L., Du, L.-J., Schuler, D.L., Cloude, S.R., 1999b. Unsupervised classification using polarimetric decomposition and the complex wishart classifier. IEEE Trans. Geosci. Remote Sens. 37 (5), 2249–2258.
Lee, J.-S., Grunes, M.R., Pottier, E., 2001. Quantitative comparison of classification capability: fully polarimetric versus dual and single-polarization SAR. IEEE Trans. Geosci. Remote Sens. 39 (11), 2343–2351.
Lee, J.-S., Grunes, M.R., Schuler, D.L., Pottier, E., Ferro-Famil, L., 2006. Scattering-model-based speckle filtering of polarimetric SAR data. IEEE Trans. Geosci. Remote Sens. 44 (1), 176–187.
Lee, J.-S., Ainsworth, T.L., Kelly, J.P., Lopez-Martinez, C., 2008. Evaluation and bias removal of multilook effect on entropy/alpha/anisotropy in polarimetric SAR decomposition. IEEE Trans. Geosci. Remote Sens. 46 (10), 3039–3052.
Lee, J.-S., Wen, J.-H., Ainsworth, T.L., Chen, K.-S., Chen, A.J., 2009. Improved sigma filter for speckle filtering of SAR imagery. IEEE Trans. Geosci. Remote Sens. 47 (1), 202–213.
Lee, J.-S., 1980. Digital image enhancement and noise filtering by use of local statistics. IEEE Trans. Pattern Anal. Mach. Intell. (2), 165–168.
Lopez-Martinez, C., Fabregas, X., 2008. Model-based polarimetric SAR speckle filter. IEEE Trans. Geosci. Remote Sens. 46 (11), 3894–3907.
Park, S.-E., Moon, W.M., 2007. Unsupervised classification of scattering mechanisms in polarimetric SAR data using fuzzy logic in entropy and alpha plane. IEEE Trans. Geosci. Remote Sens. 45 (8), 2652–2664.
Vasile, G., Trouvé, E., Lee, J.-S., Buzuloiu, V., 2006. Intensity-driven adaptive-neighborhood technique for polarimetric and interferometric SAR parameters estimation. IEEE Trans. Geosci. Remote Sens. 44 (6), 1609–1621.
Wang, Y., Davis, F., 1997. Decomposition of polarimetric synthetic aperture radar backscatter from upland and flooded forests. Int. J. Remote Sens. 18 (6), 1319–1332.
Yajima, Y., Yamaguchi, Y., Sato, R., Yamada, H., Boerner, W.-M., 2008. PolSAR image analysis of wetlands using a modified four-component scattering power decomposition. IEEE Trans. Geosci. Remote Sens. 46 (6), 1667–1673.
Yamaguchi, Y., Sato, A., Boerner, W.-M., Sato, R., Yamada, H., 2011. Four-component scattering power decomposition with rotation of coherency matrix. IEEE Trans. Geosci. Remote Sens. 49 (6), 2251–2258.
Zhong, H., Zhang, J., Liu, G., 2014. Robust polarimetric SAR despeckling based on nonlocal means and distributed lee filter. IEEE Trans. Geosci. Remote Sens. 52 (7), 4198–4210.